ELSEVIER

Journal of Alloys and Compounds 424 (2006) 237–242

Journal of ALLOYS AND COMPOUNDS

www.elsevier.com/locate/jallcom

Spectroscopic study of Praseodymium(III) bidentate nitrate dihydrate complexes: $K_2Pr(NO_3)_5(H_2O)_2$ and $K_2La_{(1-x)}Pr_x(NO_3)_5(H_2O)_2$

Karine Le Bris*, Christian Reber

Département de chimie, Université de Montréal, C.P. 6128, succursale Centre-ville Montréal, Que., Canada H3C 3J7

Received 15 June 2005; accepted 21 October 2005
Available online 8 February 2006

Abstract

The absorption and emission spectra of 4f–4f transitions of $K_2Pr(NO_3)_5(H_2O)_2$ and $K_2La_{(1-x)}Pr_x(NO_3)_5(H_2O)_2$ (with $0 < x \leq 1$) are reported for different temperatures and Pr^{3+} concentrations. The degeneracy lifting of the rare-earth ion in the crystal leads to an approximate C_3 symmetry, sub-group of a quasi-icosahedral symmetry. The influence of the Pr^{3+}–Pr^{3+} interactions on the population of the excited levels is demonstrated. Crystal field parameter calculations have been performed with 18 experimental energy levels and the results are compared to previous calculations based on fewer transitions.

Keywords: Praseodymium; Absorption spectroscopy; Luminescence; Crystal-field parameters; Bidentate nitrates; Icosahedral symmetry

1. Introduction

Numerous studies over the recent years have been focused on crystals presenting high non-linear coefficients and allowing second harmonics generation. Among them, $K_2RE(NO_3)_5(H_2O)_2$ (with RE = rare-earth) presents an interesting substitute to KDP. While the non-linear optical properties of this crystal have been the subject of various publications [1–5], its other spectroscopic properties have not yet been studied. We concentrate our work on the $K_2Pr(NO_3)_5(H_2O)_2$ (KPN) crystals, the Pr^{3+} ion presenting the advantage of owning transitions in the visible, inside a window without nitrate, water and potassium bands. Mixed crystals of $K_2La_{(1-x)}Pr_x(NO_3)_5(H_2O)_2$ (KLPN) have also been synthesized and their spectroscopic properties studied.

2. Synthesis and structure

KPN is produced, at a temperature around 50 °C, from an aqueous solution containing $Pr(NO_3)_3 \cdot 6(H_2O)$ and KNO_3 (Sigma–Aldrich) with a stoichiometric ratio of 2:1 for K^+ and Pr^{3+}, and nitric acid. Light green crystals are formed by spontaneous nucleation. KPN being hygroscopic, they must be kept in a dry and hot (50 °C) environment between experiments. It has been demonstrated [1] that, at this temperature, the crystal surface is not dehydrated.

The structure of KPN has recently been studied in the context of research on second-harmonic generation with the polar potassium rare-earth nitrates [1–5]. The rare-earth is coordinated to 12 oxygen atoms through two water molecules and five bidentate nitrate groups. One of the particularities of this crystal is that the $Pr–O_{(H_2O)}$ and $Pr–O_{(NO_3)}$ distances are approximately the same with a respective mean of 2.64 and 2.63 Å. It has been found that the PrO_{12} group is a distorted icosahedron with an exact C_2 symmetry. A representation of this coordination geometry is given in Figs. 1 and 2.

We have also obtained $K_2La_{1-x}Pr_x(NO_3)_5(H_2O)_2$ mixed crystals. These crystals have been made from solutions of $Pr(NO_3)_3 \cdot 6(H_2O)$ with LaO_3 with a Pr^{3+} concentration in solution of 5, 10 and 20%. The rest of the procedure is identical to the one for pure crystals.

3. Experimental results

3.1. Absorption spectroscopy

The absorption spectra are obtained with a Cary 5E spectrometer. The sample is set in a cryostat (Oxford CF 1204) and cooled by a

* Corresponding author.
E-mail address: karine.le.bris@umontreal.ca (K. Le Bris).

0925-8388/$ – see front matter © 2006 Elsevier B.V. All rights reserved.
doi:10.1016/j.jallcom.2005.10.091

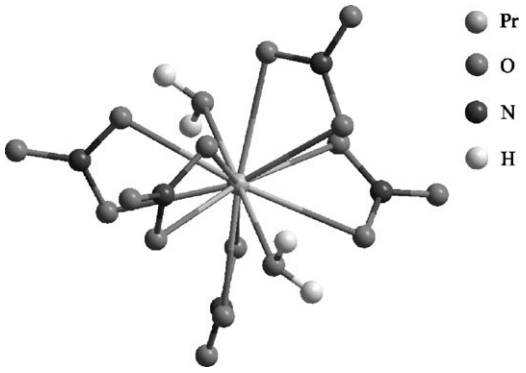

Fig. 1. Pr^{3+} ion environment in KPN.

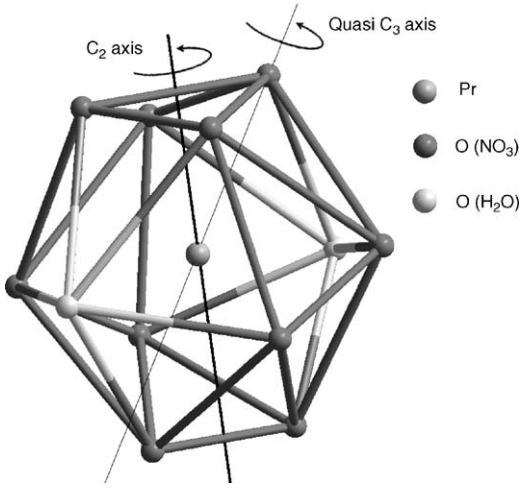

Fig. 2. Distorted icosahedral structure around the Pr^{3+} ion. The exact C_2 axis and a quasi C_3 axis are represented.

continuous flow of helium gas. An overview spectrum at low resolution (1 nm) and room temperature is presented in Fig. 3.

The transparency window opens around 350 nm. The strong absorption in the UV is attributed to the two absorption bands of the nitrate ions at 265 and 300 nm. By analogy with the spectra of Hellwig et al. [5] on $K_2RE(NO_3)_5(H_2O)_2$ with (RE = La, Ce, Pr and Nd), we can say that between 350 and 1100 nm, all the visible lines are due to f–f transitions of the Pr^{3+} ions. The lines associated to the $^3H_4 \rightarrow {}^3P_2$, $^3H_4 \rightarrow {}^3P_1$, $^3H_4 \rightarrow {}^1I_6$, $^3H_4 \rightarrow {}^3P_0$, $^3H_4 \rightarrow {}^1D_2$ and $^3H_4 \rightarrow {}^1G_4$ transitions, $^3H_4$ being the electronic ground state of the $4f^2$ configuration, are clearly visible. Beyond 1300 nm, the overlapping of the absorption bands of the nitrate and water molecules prevents the analysis of additional rare-earth transitions in the near IR.

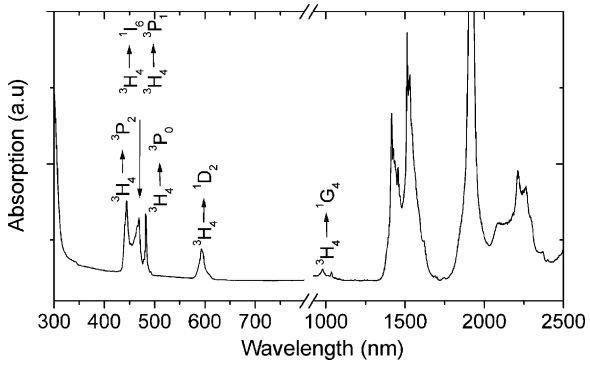

Fig. 3. KPN absorption spectra at room temperature.

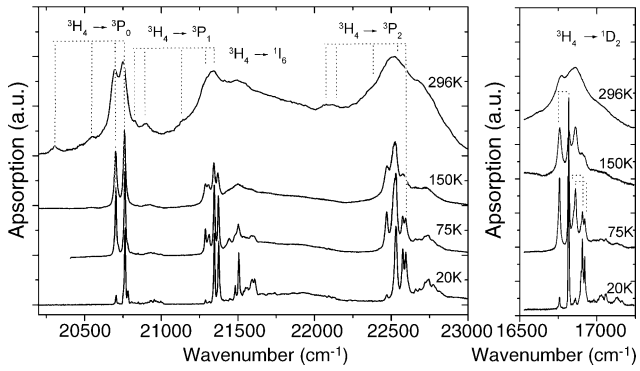

Fig. 4. High-resolution absorption spectra of the visible transitions of KPN for different temperatures. The dotted lines indicate recurrent patterns corresponding to the signature of the Stark levels of the $^3H_4$ ground state.

The $^3H_4 \rightarrow {}^3P_2$ transition is supposed to be dominant in intensity because of its hypersensitive character. The large values of the $^3H_4 \rightarrow {}^3P_0$ and $^3H_4 \rightarrow {}^3P_1$ transitions can be interpreted by a dynamic coupling polarization mechanism [6] (radiation induced ligand polarization), the transition matrix elements being close to zero in a simple static model.

High-resolution scans (Fig. 4) in the spectral regions around previously mentioned transitions show resolved structures at room temperature. To determine the vibronic or electronic nature of these lines, low temperature spectra have been measured and included in Fig. 4. The results point out without ambiguities that the observed lines correspond to transitions between the Stark components of $^3H_4$, the sub-levels of highest energy of the ground state being depopulated at low temperature. The $^3P_0$ being non-degenerate and isolated, we obtain four Stark components of $^3H_4$ at 0, 59.3, 208.8, and 446.3 cm^{-1}. These components appear as well partially on the $^3H_4 \rightarrow {}^3P_2$, $^3H_4 \rightarrow {}^3P_1$ and $^3H_4 \rightarrow {}^1D_2$ transitions. A structure is also visible on the blue wing of the $^3H_4 \rightarrow {}^3P_0$ transition and is attributed to a component of the $^3H_4 \rightarrow {}^3P_1$ transition which leads to a 5th Stark level around 550 cm^{-1}.

The influence of the quasi-icosahedral environment is marked by the number of lines obtained at low temperature. Around 20 K, where only the lowest Stark sub-level of $^3H_4$ is populated, we obtained two components for $^3P_1$ and three components for $^3P_2$ and $^1D_2$. This degree of degeneracy is consistent with a threefold symmetry axis and a C_3 point group symmetry. This symmetry group, sub-group of a perfect icosahedral symmetry, leads to the degeneracy lifting on J presented in Table 1.

The absence of line doubling demonstrates that the Pr^{3+} ion in the title compound is associated to only one symmetry site.

Polarized absorption spectroscopy does not induce distinct dichroic ratios. It is therefore impossible to experimentally assign irreducible representations to the Stark components. Several interpretations can explain this absence of polarization effects. The most likely is the

Table 1
Number of atomic states for C_3 symmetry

C_3	Number of levels
$J = 0$	1
$J = 1$	2
$J = 2$	3
$J = 3$	5
$J = 4$	6
$J = 5$	7
$J = 6$	9

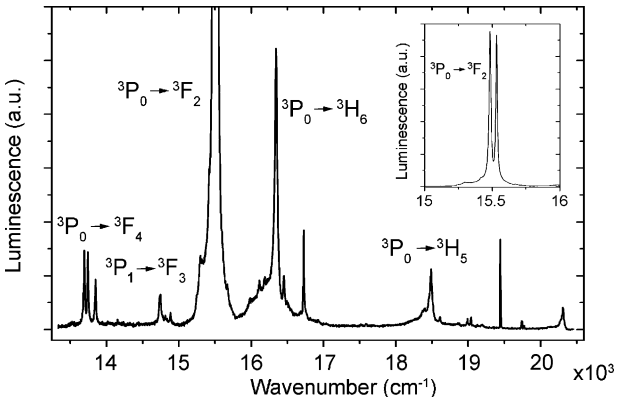

Fig. 5. Emission spectrum of $K_2Pr(NO_3)_5(H_2O)_2$ at 200 K. Inset: $^3P_0 \rightarrow {}^3F_2$ transition (structure out of scale in the main figure).

presence of multiple pseudo C_3 axes in the rare-earth environment as it can be seen in Fig. 2. Other possible causes are defects in the crystal sample or adsorbed water at the surface of the hygroscopic crystal.

3.2. Emission spectroscopy

Emission from the excited levels of Pr^{3+} ion in KPN and KLPN is weak due to the strong vibrational relaxation process existing in crystals with highly coordinated molecular ligands. To increase the detection sensitivity, we use a Raman confocal microscope (Renishaw System 3000). The sample is cooled by a liquid Helium flow in a Janis ST-500 cryostat.

The excitation source is an argon laser at 488 nm which corresponds to the red wing of the $^3H_4 \rightarrow {}^3P_0$ transition. The emitted light is collected and detected by a Peltier-cooled CCD camera. The emission spectrum obtained for a KPN crystal is presented in Fig. 5. The higher energy Stark components of $^3H_4$, which are the only ones contributing to the excitation, are depopulated at low temperature. Therefore, we cannot reach the resolution obtained in absorption spectra.

The bands assignment is done from the observed and calculated transitions on the $Pr_2Mg_3(NO_3)_{12} \cdot 24H_2O$ crystal [8] and from the Judd-Ofelt theory which predicts dominant contributions for electric dipolar transitions with $\Delta J = 2$ and magnetic dipolar transition with $\Delta J = 1$.

The strong emission lines observable between 15,000 and 17,000 cm^{-1} are attributed to electric dipolar transitions $^3P_0 \rightarrow {}^3F_2$ and $^3P_0 \rightarrow {}^3H_6$. We also observe the weaker $^3P_0 \rightarrow {}^3F_4$ and the "forbidden" $^3P_0 \rightarrow {}^3H_5$ transition.

The structure around 14,700 cm^{-1} is attributed to the hypersensitive $^3P_1 \rightarrow {}^3F_3$ transition. This assignment is based on two factors: (1) the structure is more sensitive to temperature than those of the other transitions which implies that it does not depend directly on the population of the $^3P_0$ level; (2) the calculation in Section 4.3 leads to a $^3F_3$ state between 6395.6 and 6648.5 cm^{-1} (see Table 2) which puts this structure inside the validity range of the $^3P_1 \rightarrow {}^3F_3$ transition. The populating mechanism of the $^3P_1$ level must still be investigated. The more direct explanation consists in a multiphonon excitation from $^3P_0$ to $^3P_1$. A two-photon transition or an absorption from $^3P_0$ to a 4f–5d excited state or a nitrate band are unlikely because they do not depend on the temperature.

The $^1D_2 \rightarrow {}^3H_4$ transition is not observable in KPN which implies either a strong multiphonon deexcitation of the $^3P_0$ level which pre-

Table 2
Energy levels of Pr^{3+} ions in cm^{-1} for KPN

Term	E_{exp}	E_{cal}[a]	E_{cal}[b]	Assignment
$^3H_4$	0	0	0	E
	59.3	55.7	63.0	A
	208.8	93.0	189.2	A
	208.8	103.1	205.7	E
	446.3	176.3	419.9	E
	550.0	233.0	529.9	A
$^3H_5$	*2166*	2071.5	2088.7	E
		2080.3	2099.6	A
		2084.4	2103.4	A
		2108.3	2187.7	E
		2159.5	2307.9	E
		2192.9	2378.8	E
	2286	2191.0	2416.8	A
$^3H_6$	*4044*	4080.0	3869.9	A
		4104.2	3888.0	A
		4169.6	4074.5	E
		4198.8	4218.0	E
		4244.7	4314.2	A
		4292.7	4302.5	E
		4352.9	4604.2	A
		4363.0	4550.5	E
		4444.6	4780.8	A
$^3F_2$	5237	4928.1	5254.4	E
	5285	4938.8	5290.7	E
	5285	4935.8	5234.8	A
$^3F_3$	*5886*	6217.4	6395.6	A
		6234.6	6401.1	E
		6283.4	6575.1	A
		6305.8	6648.5	A
	6029	6324.9	6645.8	E
$^3F_4$	*6923*	6905.4	6916.1	A
		6906.9	6932.5	E
		6918.6	6982.0	A
		6922.0	7009.2	E
		6922.1	7023.1	A
		6933.4	7079.2	E
$^1G_4$	*9664*	9991.0	9518.6	A
		10075.4	9603.9	E
		10189.7	9888.5	E
		10234.2	9951.5	A
		10253.2	10124.8	A
	10283	10393.1	10377.0	E
$^1D_2$	16897.6	16882.1	16856.5	E
	16906.2	16910.5	16904.5	E
	16921.9	16927.4	16933.5	A
$^3P_0$	20761.5	20761.2	20765.5	A
$^3P_1$	21345.6	21343.4	21332.3	A
	21374.4	21372.6	21365.6	E
$^1I_6$		21829.9	21498.4	A
		21863.2	21621.1	E
		21924.7	21691.2	A
		21936.7	21769.5	A
		21918.0	21770.2	E
		21948.3	21809.4	E
		22024.5	21909.2	A
		22029.0	21920.6	A
		21960.2	21874.6	E

Table 2 (*Continued*)

Term	E_{exp}	E_{cal}[a]	E_{cal}[b]	Assignment
$^3P_2$	22529.6	22539.9	22519.7	E
	22574.8	22574.1	22594.4	E
	22594.8	22579.9	22547.7	A
$^1S_4$		48717.7	47779.5	A
σ		7.13	20.8	

The levels in italics indicate estimations from the emission spectra.

[a] Calculated energies with only the 11 levels used in [8].

[b] Calculated energies with 18 levels (levels from (a) + $^3F_2$ and higher $^3H_4$ levels).

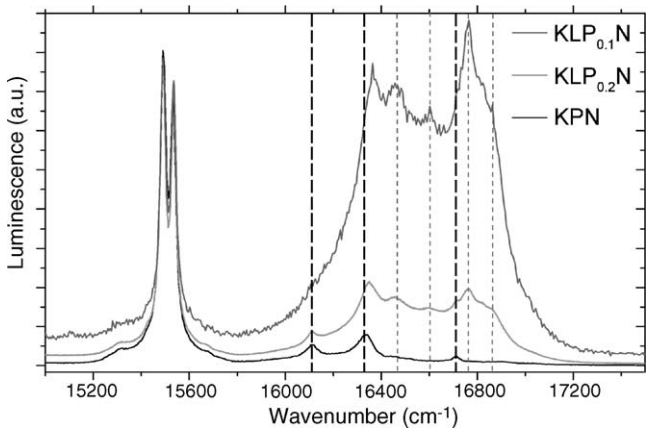

Fig. 6. Emission spectra at room temperature of KPN and KLPN (with a Pr^{3+} concentration in solution of 10 and 20%). The black dashed lines represent the visible transition in a pure crystal; the grey dotted lines, the transitions appearing in mixed crystals.

vents the efficient population of the $^1D_2$ level, or an efficient non radiative relaxation of $^1D_2$ state. A weak emission (not presented here) attributed to the $^1G_4 \rightarrow {}^3H_4$ relaxation is observable between 9760 and 10,260 cm^{-1}. The emission corresponding to the $^3P_0 \rightarrow {}^1G_4$ transition being barely observable, we can deduce that the $^1G_4$ population must come essentially from non radiative relaxation from the higher-energy $^3P_0$ and/or $^1D_2$ levels.

A fundamental difference between KPN and KLPN occurs in the emission spectra (Fig. 6) where a large spectral structure appears around the $^3P_0 \rightarrow {}^3H_6$ transition. The relative intensity of this structure increases as the Praseodymium concentration decreases. These new lines cannot come from a direct relaxation of Lanthanum, as a pure $K_2La(NO_3)_5(H_2O)_2$ crystal does not emit in this spectral region. The limitation imposed by the excitation energy, and therefore by the temperature of the experimental acquisition, prevents us to precisely determine the energy levels corresponding to these lines. Nevertheless, their position overlapping the $^3P_0 \rightarrow {}^3H_6$ transition lines allows to identify them as a relaxation from $^1D_2$ to $^3H_4$. The apparition of these bands as the concentration of Pr^{3+} decreases is linked to the variation of the mean distance between Pr^{3+} ions, and, therefore, to their interactions.

Interactions between neighboring ions of the same species had been studied through vibrational transitions (see for example [9]). Vibronic lines seemed to be enhanced as the concentration of rare-earth ions is increased. The phenomenon had been interpreted as "super-exchange" processes between two ions which promote vibronic couplings. But, it appeared later that the observed dependance in absorption spectra between concentration of rare-earth and intensities of vibronic lines could originate from a saturation effect [10].

Our observation in emission provides new evidence that interactions exist between two Pr^{3+} ions. This effect can be interpreted remembering that Pr^{3+} ions own extended 4f wave functions leading to a stronger coupling between ionic wave functions. The increase of the Pr^{3+}–Pr^{3+} distance drives a decrease of vibronic couplings and multiphonon relaxations and enables either the population of the $^1D_2$ level from the $^3P_0$ level or/and the radiative relaxation of $^1D_2$. It is interesting to note that, for an initial Praseodymium concentration of 10% in solution, the $^1D_2 \rightarrow {}^3H_4$ bands become the dominant contribution in emission.

An overview of the observable transitions in absorption and emission is presented in Fig. 7.

4. Crystal field parameters

To obtain a consistent assignment of observed electronic transitions and an evaluation of energy levels non-observable experimentally, a calculation of crystal field parameters has been made.

4.1. Theory and parametric considerations

For a f^n configuration, the total Hamiltonian can be written as the sum of the free ion contributions with the crystal field Hamiltonian considered as a small perturbation.

$$H = H_{fe} + H_{cf} \tag{1}$$

Each interaction contains a computable angular contribution and a radial contribution treated as a free parameter. For a f^2 configuration, the free ion Hamiltonian includes 14 parameters.

$$H_{fe} = E_0 + \sum_{k=2,4,6} F^k(nf, nf) f_k + \xi \sum_i \mathbf{s}_i \cdot \mathbf{l}_i + \alpha L(L+1) + \beta G(G_2) + \gamma G(R_\tau) + \sum_{i=0,2,4} m_i M^i + \sum_{i=2,4,6} p_i P^i \tag{2}$$

E_0 represents the average electronic kinetic energy. F^2, F^4 and F^6 stand for the electrostatic interaction parameters. The spin orbit coupling is represented by the parameter ξ. α, β and γ define the two-body configuration interactions parameters. M^0, M^2, M^4 represent the relativistic effects and P^2, P^4, P^6, the magnetic interactions. f_k, $\mathbf{s}_i$, $\mathbf{l}_i$, $L(L+1)$, $G(G_2)$, $G(R_\tau)$, m_i and p_i are the angular part of the operators.

The crystal field Hamiltonian is given, in the Wybourne normalization, by

$$H_{cf} = \sum_{0\le k\le 6} \sum_{0\le q\le k} B_q^k [C_q^k + (-1)^q C_{-q}^k] + i S_q^k [C_q^k - (-1)^q C_{-q}^k] \tag{3}$$

where C_q^k is the spherical tensor operator and B_q^k, S_q^k are ,respectively, the real and imaginary parts of the variable crystal field parameters.

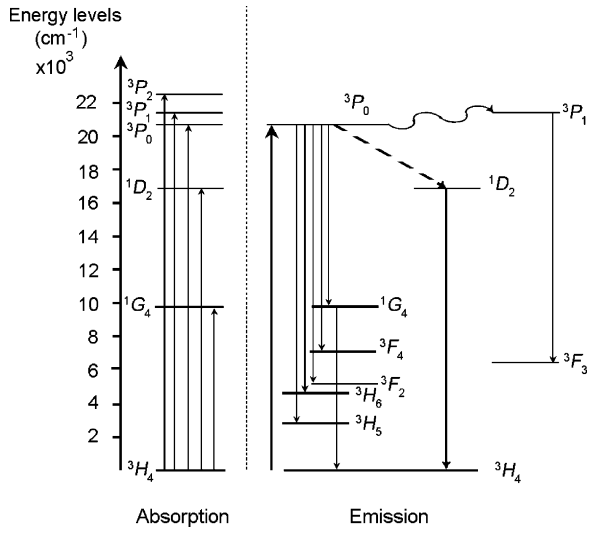

Fig. 7. Observable transitions in KPN in absorption and emission from a 488 nm laser excitation. The bold line presents the $^1D_2 \rightarrow {}^3H_4$ transition only observable in KLPN crystal. The dashed line indicates the radiative or non radiative process of populating the $^1D_2$ state.

In the previous section, we have determined that the Pr^{3+} ion presents a spectroscopic C_3 symmetry. This symmetry gives 9 variable crystal field parameters to add to the 14 free ion parameters. To reduce the number of variables, we consider, to a first approximation, the higher point group of symmetry C_{3v}. This simplification suppresses the imaginary parts S_q^k and reduces the crystal field parameters to the six terms B_0^2, B_0^4, B_3^4, B_0^6, B_3^6 and B_6^6. The M^i and P^i parameters are restrained by the ratios $M^2/M^0 = 0.56$, $M^4/M^0 = 0.38$, $P^4/P^2 = 0.75$ and $P^6/P^2 = 0.50$ [11]. A first set of parameters can be taken from the analysis of $Pr_2Mg_3(NO_3)_{12} \cdot 24H_2O$ [8]. This crystal presents a rare-earth environment similar to the one of KPN, the Pr^{3+} ion being situated in a C_3 symmetry site and surrounded by twelve oxygen atoms through six bidentate nitrate groups.

4.2. First calculation

We start our calculation by considering only the 11 levels presented in [8] to verify the similarity between the two compounds. The lack of polarization effects in KPN is an obstacle to the attribution of irreducible representations to the experimentally observed energy levels. We proceeded by analogy with the calculation of [8] for the observable transitions in absorption spectroscopy, i.e. $^3P_0$, $^3P_1$, $^3P_2$, $^1D_2$ and the first two levels of $^3H_4$. Due to the limited number of experimental levels involved, we restrained the 6th order crystal field parameters by the ratios $B_6^6/B_0^6 = -0.921$ and $B_3^6/B_6^6 = -2.360$ found in [7] for an icosahedral symmetry.

The calculated levels and the fitted parameters are presented in column (a) of Table 2 and in the first column of Table 3, respectively. We obtain a good parametric fit with values close to those found in [8] and a standard deviation of 7.1 cm^{-1}. The dominant crystal field parameters are the B^6 series, as predicted by [7]. This predominance makes difficult the evaluation of the other parameters B_0^2, B_0^4, B_3^4 which are involved in the same calculations. In particular, the B_3^4 parameter varies too much to allow a proper fit. Thus, we must keep this parameter fixed to the calculation the value determined in [8].

4.3. Second calculation

A second parametric fit including the observed $^3H_4$ and $^3F_2$ Stark levels has been carried out to obtain more precise eval-

Table 3
Free ion and crystal field parameters in cm^{-1} for KPN

Parameter	KPN with 11 levels	KPN with 18 levels	From Hens and Gorller-Walrand [8]	From Judd [7]
E_0	10093.4	10113.8		
F^2	69784.6	69453.2	69643.7	
F^4	55825.2	52187.9	54173.2	
F^6	35586.1	34206.5	34167.3	
α	(22.8)	22.9	(22.8)	
β	(−556.6)	−749.9	(−556.6)	
γ	(1371.4)	1377.7	(1371.4)	
ζ	736.1	715.7	763.4	
M^0	(−2.08)	(−2.08)	(−2.08)	
M^2	(−1.165)	(−1.165)	(−1.165)	
M^4	(−0.645)	(−0.645)	(−0.645)	
P^2	(−88.6)	(−88.6)	(−88.6)	
P^4	(−66.45)	(−66.45)	(−66.45)	
P^6	(−44.3)	(−44.3)	(−44.3)	
B_0^2	−99.4	−115.7	−172.1	−140
B_0^4	4.9	−194.4	15.2	−160
B_3^4	(28.2)	155.1	28.2	201
B_0^6	−300.8	−402.1	−268.7	−800
B_3^6	749.1	2065.3	634.2	1796
B_6^6	−317.4	−536.7	−283.5	737

A comparaison with the results for the crystal of same symmetry $Pr_2Mg_3(NO_3)_{12} \cdot 24H_2O$ from [8] and [7] is given. Numbers in parenthesis indicate fixed parameters.

uation of parameters. Except for the $^3P_0 \rightarrow {}^3F_2$ transition, the resolution is insufficient to associate Stark levels to the structures observed in emission. Nevertheless, it is possible to assign to each transition an energetic band position to test the validity of the calculation. Because of the higher number of levels involved in the calculation, we are able to treat α, β, γ and B_3^4 parameters as free and to remove the constant ratio between the B^6 series.

The calculated energy levels from the 18 experimental energy levels are presented in column (b) of Table 2 and the corresponding set of parameters is presented in the second column of Table 3. The standard deviation of this parametric fit is 20.8 cm^{-1}. The new calculation changes considerably the crystal field parameters. We observe a large absolute increase of all the values particularly in the 6th order. The stronger crystal field is induced by the splitting of the ground state, far larger than the one obtained in the first calculation. It is noticeable that the new crystal field parameters are closer to those obtained theoretically by Judd [7] than to those obtained by analysis of experimental spectra in [8]. The new ratios between the 6th order parameters are $B_6^6/B_0^6 = 1.335$ and $B_3^6/B_6^6 = 3.848$. The variation of the ratios can be interpreted by the discrepancy between our quasi-icosahedral structure and a perfect I_h symmetry.

The difference between the two calculations underlines the difficulties to obtain an accurate crystal field representation with few experimental levels. To validate our new parameters, it is still necessary to provide more data. For that purpose, emission spectra at low temperature are required in order to provide more resolved transitions and proceed to a valuable parametric fit. That being said, we can already see that our new calculated levels reproduce very well the energy ranges of the $^3H_5$, $^3H_6$, $^3F_3$, $^3F_4$ and $^1G_4$ levels.

Divergence still remains between calculated and experimental levels. These mismatches could come from the fixed parameters or the approximation of a C_{3v} symmetry. As it was already pointed out, more experimental levels are required to proceed to a more accurate parametric fit. A calculation including the coupling between 4f–4f and 4f–5d levels could also improve the results.

5. Conclusions

Absorption and emission spectra of KPN and KLPN crystals have been carried out. These studies provide a first report of the Pr^{3+} ion energy levels in these crystals. The observed degeneracy lifting shows that the dominant symmetry of the rare-earth environment is a C_3 point group symmetry. This observation meets the projection of Judd [7] on the double nitrate compounds.

The analysis of mixed KLPN crystals shows resolved structure around the $^3P_0 \rightarrow {}^3H_6$ transition. This structure, very sensitive to the Pr^{3+} ion concentration, is attributed to the $^1D_2 \rightarrow {}^3H_4$ relaxation and underlines the essential importance of Pr–Pr interactions.

Parametric calculations have been performed. The results allow us to confirm that the structures around 15,000 cm^{-1} come from the relaxation of the $^3P_1$ state toward the $^3F_3$ level. We also pointed out the importance to include a sufficient number of experimental levels in order to obtain accurate evaluation of crystal field parameters.

References

[1] C.A. Ebbers, L. Davis DeLoach, M. Webb, D. Eimerl, S.P. Velsko, D.A. Keszler, IEEE J. Quant. Electron. 29 (1993) 497–507.
[2] H. Zhuo, C. Fang, W. Qingwu, Y. Zhaohe, Chin. Sci. Bull. 40 (12) (1994) 997.
[3] W. Dong, H. Zhang, Q. Su, Y. Lin, S. Wang, C. Zhu, J. Solid State Chem. 148 (1999) 302–307.
[4] P. Held, H. Hellwig, S. Ruhle, L. Bohaty, J. Appl. Crystallogr. 33 (2000) 372–379.
[5] H. Hellwig, S. Ruhle, P. Held, L. Bohaty, J. Appl. Crystallogr. 33 (2000) 380–386.
[6] C.K. Jørgensen, B.R. Judd, Mol. Phys. 8 (1964) 281–290.
[7] B.R. Judd, Proc. R. Soc. A 232 (1955) 458–474.
[8] E. Hens, G. Gorller-Walrand, J. Alloys Compd. 225 (1995) 66–70.
[9] A. Meijerink, C. de Mello Donega, A. Ellens, J. Sytsma, G. Blasse, J. Lumin. 58 (1–6) (1994) 26–32.
[10] C. de Mello Donega, A. Meijerink, G. Blasse, J. Lumin. 62 (5) (1994) 189–201.
[11] H.M. Crosswhite, H. Crosswhite, J. Opt. Soc. Am. B 1 (2) (1984) 246–254.